Monografías Matemáticas *García de Galdeano* **43**, 151–160 (2024)

# COMPUTING BUOYANCY FLOWS WITH STABILIZED FINITE ELEMENT METHODS: THE BOUSSINESQ APPROACH VERSUS THE FULL NAVIER-STOKES EQUATIONS

Guillermo Hauke and Jorge Lanzarote

**Abstract.** This paper compares two models to simulate buoyancy flows, set in a non-standard computational framework. The models are the Boussinesq model and the general divariant fluid model. In both cases, the set of equations respects the second-law of thermodynamics. The numerical framework is based on a unified approach to compute compressible and incompressible flows, which solves the total energy equation and it is numerically conservative. Numerical examples show that the general divariant fluid model is competitive for problems with small temperature differences, whereas it is advantageous for large temperature differences. Finally, VMS adaptivity is shown to accelerate convergence with respect to number of degrees of freedom.

*Keywords:* buoyant flows, Boussinesq approximation, stabilized method, SUPG, SGS, compressible/incompressible formulation, VMS adaptivity.

*AMS classification:* 76D05, 65M60.

## §1. Two models for buoyancy flows

Buoyancy flows have many important practical applications in the world of climatization, indoor ventilation and indoor comfort, and many other fluid flow problems driven by temperature differences. Since the beginning of numerical methods, every existing method has been applied to this problem and, therefore, the scientific literature is really vast (a short review of articles dealing with this problem can be found in [15]).

This work compares two models for the simulation of low-speed buoyant flows: one based on the generalized liquid/gas thermodynamical model and the other one based on the Boussinesq approximation. In both cases the flow dynamics is given by the Navier-Stokes equations including an energy or temperature equation. In the present case, the method departs from the unified approach to compute compressible and incompressible flows exposed in [12, 13, 15], which uses the total energy equation, that is, in Cartesian coordinates

$$\begin{aligned}
&\frac{\partial \rho}{\partial t} + (\rho\, u_i)_{,i} = 0 \\
&\frac{\partial \rho u_i}{\partial t} + (\rho u_i u_j)_{,j} = -p_{,i} + \tau'_{ij,j} + \rho f_{mi} \\
&\frac{\partial \rho(e + \frac{1}{2}u^2)}{\partial t} + \left(\rho(e + \frac{1}{2}u^2)u_j\right)_{,j} = -(pu_i)_{,i} + (\tau'_{ij}u_i)_{,j} + \rho f_{mi}u_i - q_{i,i} + \dot{q}_v
\end{aligned} \tag{1}$$

where $\rho$ is the density, $u_i$ the Cartesian velocity components, $p$ the pressure, $\tau'_{ij}$ the components of the viscous stress tensor, $f_{mi}$ the body force term, $e$ the specific internal energy, $q_i$ the heat flux vector components and $\dot{q}_v$ the volumetric heat source.

In vector form, the above system of equations can be written as

$$\mathbf{U}_{,t} + \mathbf{F}^{\text{adv}}_{i,i} = \mathbf{F}^{\text{diff}}_{i,i} + \mathbf{S} \tag{2}$$

where $\mathbf{U}$ is the vector of conservation variables, $\mathbf{F}^{\text{adv}}_i$ the $i$-th Euler Jacobian, $\mathbf{F}^{\text{diff}}_i$ the $i$-th diffusive flux and $\mathbf{S}$ the source vector.

## 1.1. Generalized fluid model

Real fluids (even incompressible liquids) display compressible behavior and, therefore, their density is a function of temperature and pressure. One way of modeling the equation of state of such fluids is through the model of a general divariant substance, in which the thermodynamic variables depend on two independent thermodynamic variables. In [3, 12, 13] the thermodynamic variables are taken as the compressibility coefficients at constant pressure $\alpha_p$ and at constant temperature $\beta_T$,

$$\beta_T = \frac{1}{\rho}\left(\frac{\partial \rho}{\partial p}\right)_T \qquad \alpha_p = -\frac{1}{\rho}\left(\frac{\partial \rho}{\partial T}\right)_p \tag{3}$$

This model has non-standard features for the simulation of buoyancy flows, which endowed the method with important advantages:

(i) As explained in the unified approach of [12, 13], the present model is based on the conservative form of the transport equations and it uses the total energy equation instead of the temperature equation. Thus, the finite element method that emanates from is conservative.

(ii) This model is valid for any temperature gradient (compare to the Boussinesq model, which holds up to relative temperature variations of about 10%[8]).

(iii) As shown in [3, 12, 13, 14, 15] this model satisfies the second law of thermodynamics. This is specially relevant, since many of the models for buoyancy driven flows violate this principle [23, 24]. Another important consequence of this property is that entropy stability can be inherited at the discrete level by the numerical formulation.

(iv) Regarding the continuity equation [9], in the present model the flow divergence may be non-vanishing. Therefore, it is not approximated as zero, as in the Boussinesq model.

## 1.2. Boussinesq model

In this model, the fluid is assumed incompressible, that is, of constant density $\rho_0$ and, therefore, the effect of density variations is accounted for in the source terms. In particular, the gravity forcing term is substituted by the buoyant forces with respect to equilibrium,

$$\mathbf{f}_m = -\mathbf{g}\alpha_p(T - T_0) \tag{4}$$

where $\mathbf{g}$ is the gravity acceleration, $\rho = \rho_0$ is the density at the reference temperature $T_0$ and $\alpha_p$ is the thermal expansion coefficient at constant pressure. Note that in this model $p$ is the departure from the equilibrium hydrostatic pressure [20]. It is interesting to remark the following ideas.

(i) The entropy production of the buoyancy terms in the Boussinesq model should cancel because gravity is a conservative field. Indeed, this is satisfied by the present model. However, there are Boussinesq implementations that do not respect entropy production [23, 24], which leads to physically wrong solutions [14]. From the numerical point of view this is also an important property because the present formulation inherits stability from the discrete second law of thermodynamics.

(ii) This model neither suffers the entropy production pitfall related to the absence of the expansion power in the temperature or internal energy equation [23, 24].

## §2. Stabilized formulation

Using any well-defined set of variables $\mathbf{Y}$, it is possible to rewrite (2) in quasi-linear form as

$$\mathbf{A}_0\mathbf{Y}_{,t} + \mathbf{A}_i\mathbf{Y}_{,i} = (\mathbf{K}_{ij}\mathbf{Y}_{,j})_{,i} + \mathbf{S} \tag{5}$$

where $\mathbf{A}_0 = \mathbf{U}_{,\mathbf{Y}}$, $\mathbf{A}_i = \mathbf{F}^{\text{adv}}_{i,\mathbf{Y}}$ is the $i$th Euler Jacobian matrix, and $\mathbf{K} = [\mathbf{K}_{ij}]$ is the diffusivity matrix where $\mathbf{K}_{ij}\mathbf{Y}_{,j} = \mathbf{F}^{\text{diff}}_i$.

In this paper, special attention is paid to the choice of pressure primitive variables,

$$\mathbf{Y} = \begin{Bmatrix} p \\ \mathbf{u} \\ T \end{Bmatrix} \tag{6}$$

with $p$ the pressure, $u_i$ the Cartesian velocity components and $T$ the absolute temperature. The matrices and vectors for these variables can be found in [13]. This set of variables is endowed with the property that the incompressible limit is well behaved.

The quasi-linear form can be written as

$$\mathcal{L}\mathbf{Y} = \mathbf{S}_0 \tag{7}$$

with the differential operators defined below

$$\begin{aligned} \mathcal{L}\mathbf{Y} &= \mathbf{A}_0\mathbf{Y}_{,t} + \mathbf{A}_i\mathbf{Y}_{,i} - (\mathbf{K}_{ij}\mathbf{Y}_{,j})_{,i} - \mathbf{C}\mathbf{Y} \\ \mathcal{L}^T\mathbf{Y} &= \mathbf{A}_0^T\mathbf{Y}_{,t} + \mathbf{A}_i^T\mathbf{Y}_{,i} - (\mathbf{K}_{ij}^T\mathbf{Y}_{,i})_{,j} - \mathbf{C}^T\mathbf{Y} \\ -\mathcal{L}^*\mathbf{Y} &= \mathbf{A}_0^T\mathbf{Y}_{,t} + \mathbf{A}_i^T\mathbf{Y}_{,i} + (\mathbf{K}_{ij}^T\mathbf{Y}_{,i})_{,j} + \mathbf{C}^T\mathbf{Y} \\ \mathcal{L}^T_{\text{SUPG}}\mathbf{Y} &= \mathbf{A}_i^T\mathbf{Y}_{,i} \end{aligned} \tag{8}$$

and the source term written as

$$\mathbf{S} = \mathbf{C}\mathbf{Y} + \mathbf{S}_0 \tag{9}$$

Note that the difference between $\mathcal{L}^T$ and $-\mathcal{L}^*$ is the sign of the diffusive and source terms.

In this paper, the time-discontinuous space-time Streamline Upwind Petrov-Galerkin (SUPG) and Subgrid-Scale (SGS) stabilized methods [2, 26] are considered. In the absence of source terms and for linear shape functions both methods coincide.

Consider a space-time domain, where the time interval $I = ]0, T[$ is subdivided into $N$ intervals $I_n = ]t_n, t_{n+1}[$, $n = 0, 1, \ldots, N-1$. We define for each time interval $Q_n = \Omega \times I_n$ and $P_n = \Gamma \times I_n$, where $\Omega$ is the spatial domain and $\Gamma$ its boundary. Finally, the "slab" $Q_n$ is decomposed into elements $Q_n^e$, $e = 1, 2, \ldots, (n_{\text{el}})_n$.

Following [12, 13] the variational formulation is defined for the set of variables $\mathbf{Y}$. Within each $Q_n$, $n = 0, 1, \ldots, N-1$, find $\mathbf{Y} \in \mathcal{S}_{\mathbf{Y}}$ such that $\forall\, \mathbf{W} \in \mathcal{V}_{\mathbf{Y}}$ :

$$\begin{aligned}
&\int_{Q_n} \Big( -\mathbf{W}_{,t} \cdot \mathbf{U}(\mathbf{Y}) - \mathbf{W}_{,i} \cdot \mathbf{F}_i^{\text{adv}}(\mathbf{Y}) + \mathbf{W}_{,i} \cdot \mathbf{K}_{ij} \mathbf{Y}_{,j} - \mathbf{W} \cdot \mathbf{S} \Big) dQ \\
&\quad + \int_{\Omega} \Big( \mathbf{W}(t_{n+1}^-) \cdot \mathbf{U}(\mathbf{Y}(t_{n+1}^-)) - \mathbf{W}(t_n^+) \cdot \mathbf{U}(\mathbf{Y}(t_n^-)) \Big) \mathrm{d}\Omega \\
&\qquad + \sum_{e=1}^{(n_{\text{el}})_n} \int_{Q_n^e} \Big( \mathbb{L}\mathbf{W} \Big) \cdot \boldsymbol{\tau} \Big( \boldsymbol{\mathcal{L}} \mathbf{Y} - \mathbf{S} \Big) dQ \\
&\qquad = \int_{P_n} \mathbf{W} \cdot \Big( -\mathbf{F}_i^{\text{adv}}(\mathbf{Y}) + \mathbf{F}_i^{\text{diff}}(\mathbf{Y}) \Big) n_i dP
\end{aligned} \tag{10}$$

The first and last integrals constitute the Galerkin terms expressed as a function of the variables $\mathbf{Y}$, again written in conservative form to ensure that the weak solution is bestowed with the correct Rankine-Hugoniot relations. The jump term is written with the help of the right and left limits,

$$W(t_n^{\pm}) = \lim_{\epsilon \to 0^{\pm}} W(t_n + \epsilon) \tag{11}$$

The stabilizing term is written in terms of the differential operators $\boldsymbol{\mathcal{L}}$ and $\mathbb{L}$, which have been defined previously. According to the choice of $\mathbb{L}$, Table 1 shows the finite element methods that can be recovered.

Table 1: Relation between differential operator and type of stabilized method.

| | SUPG | GLS | SGS |
|---|---|---|---|
| $\mathbb{L}$ | $\boldsymbol{\mathcal{L}}_{\text{SUPG}}^T$ | $\boldsymbol{\mathcal{L}}^T$ | $-\boldsymbol{\mathcal{L}}^*$ |

In the case that the source term is independent of the unknown variables and the shape functions are linear, $-\boldsymbol{\mathcal{L}}^* = \boldsymbol{\mathcal{L}}_{\text{SUPG}}^T = \boldsymbol{\mathcal{L}}^T$. Note that when entropy variables are used, $\widetilde{\boldsymbol{\mathcal{L}}} = \widetilde{\boldsymbol{\mathcal{L}}}^T$ because of the symmetry of the coefficient matrices and the symmetric form is recovered.

We assume

$$\boldsymbol{\tau} = \mathbf{Y}_{,\mathbf{V}}\, \widetilde{\boldsymbol{\tau}} \tag{12}$$

where $\widetilde{\boldsymbol{\tau}}$ is the stabilization matrix for entropy variables [17, 26]. For definitions of the $\boldsymbol{\tau}$ matrix for low-speed flows based on primitive variables see the comments and references in [15].

Note that the discontinuity-capturing operator has been omitted since we are dealing with low-speed flows [18].

# §3. Numerical examples

## 3.1. Preliminaries

In order to solve compressible and incompressible flows with the same solver, in this work the set of pressure primitive variables is chosen, $\mathbf{Y} = (p, \mathbf{u}, T)^T$

For the numerical examples presented below, the full Navier-Stokes (full NS) model uses the perfect gas equation of state. For the Boussinesq model, this equation of state is substituted by constant density. Note that the equation of state $\rho = \rho(T)$, would yield an approximated acoustically filtered compressible equations [20].

In this work, the following stabilization matrices are analyzed and compared: i)The compressible "classic" tau matrix transformed into pressure primitive variables [26, 13]; ii) The incompressible non-diagonal tau [13], referred here as HH, also an extension of [6]; iii) The incompressible Polner tau, which is an extension of the above definition, with the parameter $\omega = 0.6$ [22]. The incompressible taus defined above have been updated with the newer continuity stabilization parameter, $\tau_c$, based on the inverse of the momentum stabilization parameter, $\tau_m$. See [15] and references therein for more details.

## 3.2. Buoyancy driven square cavity

The purpose of this section is to compare, from the computational point of view, three simulation strategies: the full Navier-Stokes equations (solved with the SUPG method) and the Boussinesq model solved with the SUPG and SGS methods.

The definition of this problem is taken from [4, 19]. The flow in a closed squared cavity is impulsed by temperature difference between the vertical walls (see Fig.1). The dimensionless parameters that govern this problem are the temperature semi-difference,

$$\epsilon = \frac{T_h - T_c}{T_h + T_c} = \frac{\Delta T}{2T_0} \tag{13}$$

and the Rayleigh number, defined as

$$\mathrm{Ra} = \frac{2\epsilon g L^3}{\nu_0 \alpha_0} = \frac{g\beta \Delta T L^3}{\nu_0 \alpha_0} \tag{14}$$

where the last expression is used for the Boussinesq model. Above, $T_0 = (T_h + T_c)/2$ is the average vertical walls temperature and the subindex 0 denotes the variables computed at $T_0$. Here $\nu = \mu/\rho$ stands for the kinematic viscosity, and $\alpha = \kappa/(\rho c_p)$, the thermal diffusivity. The above definitions usually are written as a function of $\beta = \alpha_p$,

The Boussinesq model, which gives anti-symmetric solutions, is valid up to $\epsilon < 0.1$ [8]. For larger temperature differences one can talk about large temperature differences and the full Navier-Stokes equations or a low Mach number model should be used [1, 16, 7].

Two temperature differences are considered in this section, $\epsilon = 0.01$ and $\epsilon = 0.6$. The fluid is air with $\mathrm{Pr} = 0.71$. Quadrilateral bilinear elements are employed for this test case. Benchmark solutions for these cases can be found in [4, 5, 27, 1, 16, 28, 19, 21].

The baseline test case is run in a $70 \times 70$ uniform mesh with $\Delta t = 0.1$, a Generalized minimal Residual (GMRES) tolerance of $10^{-8}$ with a maximum of 60 iterations with 9 restarts,

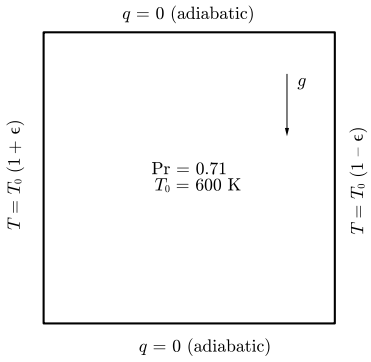


Figure 1: Buoyancy driven square cavity. Problem setup.

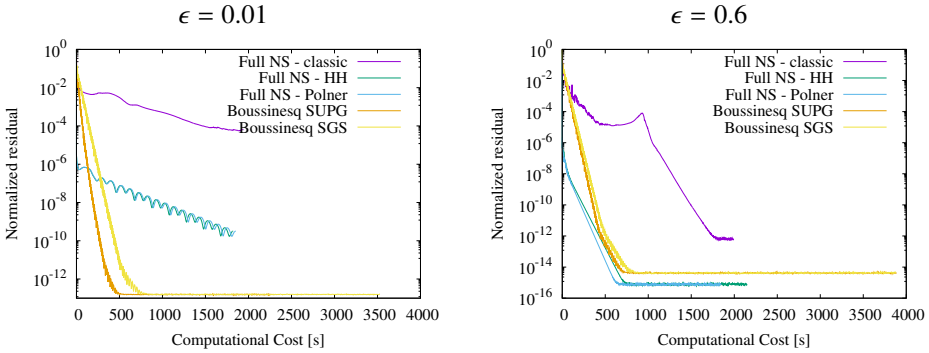


Figure 2: Buoyancy driven square cavity. Comparative study of residual convergence for various simulation strategies

and an ILU preconditioner. The classic tau allowed a larger time step for $\epsilon = 0.6$, so a value of $\Delta t = 1.0$ was chosen for this case. The viscosity has been assumed constant.

Fig. 2 compares residual convergence for the models and methods. For the Boussinesq model, both SUPG and SGS, with either the HH and the Polner taus behaved similarly, perhaps SUPG showing faster convergence than SGS for small $\epsilon$. Regarding the full Navier-Stokes equations, both HH and the Polner tau behaved identically and produce a faster convergence than the classic tau, although the classic tau improves convergence as the temperature difference is increased. Note that for the same computing parameters and small $\epsilon$, the Boussinesq model converges faster than the full Navier-Stokes equations. This advantage tends to disappear as $\epsilon$ is increased. Tables 2 and 3 compare the Nusselt numbers calculated with the present simulation strategies compared to several benchmarks.

Finally, Figs. 3 and 4 show how VMS-adapted meshes [10, 11] can speed convergence of the Nusselt number with a lesser amount of nodes and elements (see [15] for more details).

Table 2: Nusselt numbers along hot vertical wall. Ra = $10^6$, $\epsilon = 0.01$, constant $\mu$. Present methods on a $140 \times 140$ uniform mesh with various taus.

| Reference solution | $\overline{\text{Nu}}$ | $\text{Nu}_{\text{min}}$ | $\text{Nu}_{\text{max}}$ |
|---|---|---|---|
| vahl Davis [4] | 8.817 | 0.989 | 17.925 |
| Le Quéré [25] | 8.8252 | 0.97946 | 17.5360 |
| Vierendeels [27] | 8.8257 | | |
| Masud [29] | 8.81490 | | |

| Present method | tau | $\overline{\text{Nu}}$ | $\text{Nu}_{\text{min}}$ | $\text{Nu}_{\text{max}}$ |
|---|---|---|---|---|
| Full NS | Classic | 8.0833 | 0.803 | 13.932 |
| Full NS | HH | 8.8524 | 0.984 | 17.704 |
| Full NS | Polner | 8.8526 | 0.984 | 17.703 |
| Boussinesq SUPG | HH | 8.8540 | 0.982 | 17.689 |
| Boussinesq SUPG | Polner | 8.8542 | 0.982 | 17.688 |
| Boussinesq SGS | HH | 8.8632 | 0.985 | 17.704 |
| Boussinesq SGS | Polner | 8.8634 | 0.985 | 17.703 |

Table 3: Nusselt numbers along hot vertical wall. Ra = $10^6$, $\epsilon = 0.6$, Sutherland viscosity. Present methods on a $140 \times 140$ uniform mesh.

| Reference solution | $\overline{\text{Nu}}$ | $\text{Nu}_{\text{min}}$ | $\text{Nu}_{\text{max}}$ |
|---|---|---|---|
| Vierendeels et al. [28, 21] | 8.6866 | 1.0667 | 20.2704 |
| Heuveline [16, 21] | 8.6861 | 1.0674 | 20.3051 |
| Becker-Braak [1] | 8.6866 | | |

| Present method | tau | $\overline{\text{Nu}}$ | $\text{Nu}_{\text{min}}$ | $\text{Nu}_{\text{max}}$ |
|---|---|---|---|---|
| Full NS | Classic | 8.6227 | 1.027 | 17.940 |
| Full NS | HH | 9.1134 | 1.093 | 21.629 |
| Full NS | Polner | 9.1142 | 1.093 | 21.632 |

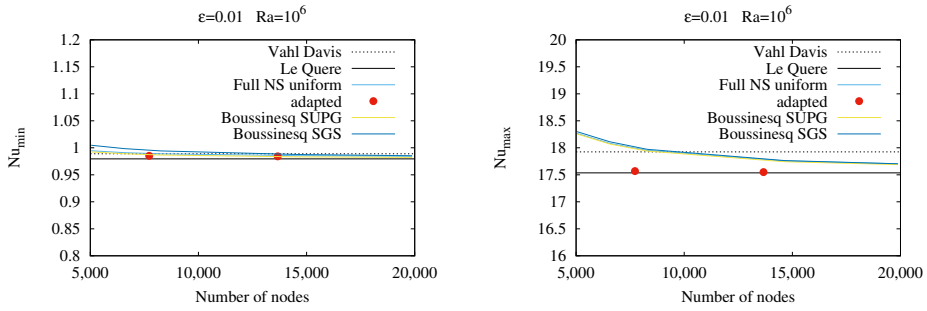


Figure 3: Buoyancy driven square cavity. Adapted solutions for $\epsilon = 0.01$ obtained with various methods and the HH tau.

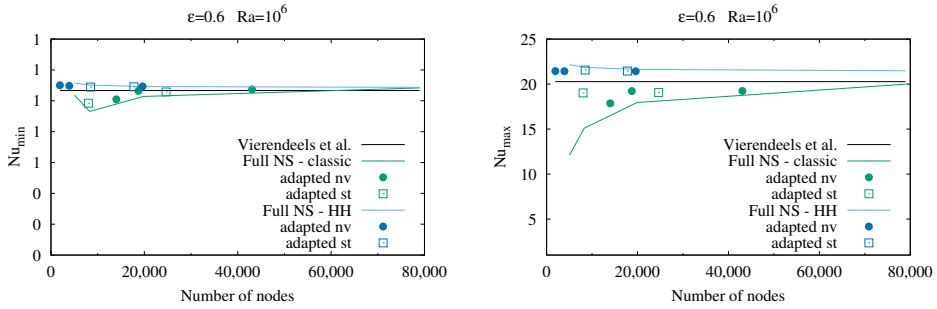


Figure 4: Buoyancy driven square cavity. Nusselt numbers along hot vertical wall for $\epsilon = 0.6$ and Sutherland viscosity for adapted meshes.

## §4. Conclusion

Two stabilized methods (SUPG and SGS) have been applied to two models for buoyancy flows, namely, the Boussinesq model and the full Navier-Stokes equations with the general divariant fluid model. Convergence, computational cost and accuracy have been analyzed and compared. The conclusion is that SUPG and SGS behave similarly, both in accuracy and residual convergence. The Boussinesq model may convergence faster than the full Navier-Stokes equations for small temperature differences, but as the temperature gradients increase, the model based on the full Navier-Stokes equations remains valid and its computational cost reduces to similar values than that of the Boussinesq model.

Finally, adaptivity based on VMS has been applied to the thermally driven cavity, showing to accelerate convergence with respect to number of nodes for the maximum and minimum Nusselt numbers.

## Acknowledgements

This work has been partially funded by the Ministerio de Economia y Competitividad under contract PID2019-106099RB-C44 (AEI/FEDER,UE), Gobierno de Aragon/FEDER-UE (Grupo de Investigacion de Referencia de Mecanica de Fluidos Computacional T32 20R).

## References

[1] Becker, R., and Braak, M. Solution of a stationary benchmark problem for natural convection with large temperature difference. *Int. J. Therm. Sci. 41* (2002), 428–439.

[2] Brooks, A., and Hughes, T. Streamline upwind/Petrov-Galerkin formulations for convection dominated flows with particular emphasis on the incompressible Navier-Stokes equations. *Comput. Meth. Appl. Mech. Engrng. 32* (1982), 199–259.

[3] Chalot, F., Hughes, T., and Shakib, F. Symmetrization of conservation laws with entropy for high-temperature hypersonic computations. *Computing Systems in Engineering 1* (1990), 459–521.

[4] de Vahl Davis, G. Natural convection of air in a square cavity: a bench mark numerical solution. *Int. J. Num. Meth. Fluids 3* (1983), 249–264.

[5] de Vahl Davis, G., and Jones, I. Natural convection in a square cavity: a comparison exercise. *Int. J. Num. Meth. Fluids 3* (1983), 227–248.

[6] Franca, L., and Frey, S. Stabilized finite element methods: II. the incompressible Navier-Stokes equations. *Comput. Meth. Appl. Mech. Engrng. 99* (1992), 209–233.

[7] Gravemeier, V., and Wall, W. Residual-based variational multiscale methods for laminar, transitional and turbulent variable-density flow at low Mach number. *Int. J. Num. Meth. Fluids 65* (2011), 1260–1278.

[8] Hamimid, S., Guellal, M., and Bouafia, M. Numerical study of natural convection in a square cavity under non-Boussinesq conditions. *Thermal Science 20*, 5 (2016).

[9] Hauke, G. *An introduction to fluid mechanics and transport phenomena*. Springer Science+Business Media, B.V., Berlin/Heidelberg, Germany, 2008.

[10] Hauke, G., Doweidar, M. H., and Miana, M. Proper intrinsic scales for a-posteriori multiscale error estimation. *Comput. Meth. Appl. Mech. Engrng 195* (2006), 3983–4001.

[11] Hauke, G., Fuster, D., and Lizarraga, F. Variational multiscale a posteriori error estimation for systems: The Euler and Navier–Stokes equations. *Computer Methods in Applied Mechanics and Engineering 283* (2015), 1493–1524.

[12] Hauke, G., and Hughes, T. A unified approach to compressible and incompressible flows. *Comput. Meth. Appl. Mech. Engrg. 113* (1994), 389–395.

[13] Hauke, G., and Hughes, T. A comparative study of different sets of variables for solving compressible and incompressible flows. *Comput. Meth. Appl. Mech. Engrg. 153* (1998), 1–44.

[14] Hauke, G., Landaberea, A., Garmendia, I., and Canales, J. On the thermodynamics, stability and hierarchy of entropy functions in fluid flow. *Comput. Meth. Appl. Mech. Engrg. 195* (2006), 4473–4489.

[15] Hauke, G., and Lanzarote, J. Simulation of low-speed buoyant flows with a stabilized compressible/incompressible formulation: The full Navier-Stokes approach versus the Boussinesq model. *Algorithms 15*, 278 (2022), 1–24.

[16] Heuveline, V. On higher-order mixed fem for low mach number flows: application to a natural convection benchmark problem. *Int. J. Num. Meth. Fluids 41* (2003).

[17] Hughes, T., Franca, L., and Hulbert, G. A new finite element formulation for computational fluid dynamics: VIII. The Galerkin/least-squares method for advective-diffusive equations. *Comput. Meth. Appl. Mech. Engrg. 73* (1989), 173–189.

[18] Hughes, T., Scovazzi, G., and Tezduyar, T. Stabilized methods for compressible flows. *J. Sci. Comput. 43* (2010), 343–368.

[19] LeQuéré, P., Weisman, C., Paillère, H., JanVierendeels, Dick, E., Becker, R., Braack, M., and Locke, J. Modelling of natural convection flows with largetemperature differences: A benchmark problem for low machnumber solvers. Part 1. Reference solutions. *ESAIM: Mathematical Modelling and Numerical Analysis 39*, 3 (2005), 609–616.

[20] Martinez, M., and Gartling, D. A finite element method for low-speed compressible flows. *Comput. Meth. Appl. Mech. Engrg. 193* (2004), 1959–1979.

[21] Paillère, H., Le LeQuéré, P., Weisman, C., Vierendeels, J., Dick, E., Braack, M., Dabbene, F., Beccantini, A., Studer, E., Kloczko, T., and et al. Modelling of natural convection flows with largetemperature differences: A benchmark problem for low machnumber solvers. Part 2. Contributions to the 2004 june conference. *ESAIM: Mathematical Modelling and Numerical Analysis 39*, 3 (2005), 617–621.

[22] Polner, M., van der Vegt, J., and van Damme, R. Analysis of stabilization operators for Galerkin least-squares discretizations of the incompressible Navier-Stokes equations. *Comput. Meth. Appl. Mech. Engrg. 196* (2006), 982–1006.

[23] Pons, M., and Quéré, P. L. An example of entropy balance in natural convection, Part 1: The usual Boussinesq equations. *Comptes Rendus Mécanique 333*, 2 (2005), 127 – 132.

[24] Pons, M., and Quéré, P. L. An example of entropy balance in natural convection, Part 2: The thermodynamic Boussinesq equations. *Comptes Rendus Mécanique 333*, 2 (2005), 133 – 138.

[25] Quéré, P. L. Accurate solutions to the square thermally driven cavity at high rayleigh number. *Computers & Fluids 20*, 1 (1991), 29 – 41.

[26] Shakib, F., Hughes, T., and Johan, Z. A new finite element formulation for computational fluid dynamics: X. The compressible Euler and Navier-Stokes equations. *Comput. Meth. Appl. Mech. Engrg. 89* (1991), 141–219.

[27] Vierendeels, J., Merci, B., and Dick, E. Numerical study of natural convective heat transfer with large horizontal temperature differences. *Int. J. Num. Meth. for Heat & Fluid Flow 11*, 4 (2001), 329–341.

[28] Vierendeels, J., Merci, B., and Dick, E. Benchmark solutions for the natural convective heat transfer problem in a square cavity with large horizontal temperature differences. *Int. J. Num. Meth. for Heat & Fluid Flow 13*, 8 (2003), 1057–1078.

[29] Zhu, L., Goraya, S., and Masud, A. A variational multiscale method for natural convection of nanofluids. *Mech. Res. Commun.* (2022).

G. Hauke
Instituto de Ingeniería de Aragón—Universidad de Zaragoza,
Area de Mecánica de Fluidos
Escuela de Ingeniería y Arquitectura
C/María de Luna 3, 50018 Zaragoza, Spain
ghauke@unizar.es

J. Lanzarote
Repsol, DE Química
C/Mendez Alvaro, 44, 28045 Madrid, Spain
jlanzaroteo@repsol.com